PHYSICAL REVIEW D **84,** 096001 (2011)

Reconstructing the heavy resonance at hadron colliders

Chan Beom Park

Instituto de Física Teórica UAM/CSIC, Nicolás Cabrera 13-15, Universidad Autónoma de Madrid, Cantoblanco, 28049 Madrid, Spain

(Received 18 July 2011; published 4 November 2011)

We investigate the method for constructing the invariant mass using the M_{T2}-assisted on-shell (MAOS) approximation to the invisible particle momenta in the cascade decays of a new particle resonance produced at hadron colliders. We note that the MAOS reconstruction can be defined in several different ways, while keeping the efficiency of approximation at a similar level, and one of them provides a unique solution for each event. It is shown that the invariant mass distribution constructed with the MAOS momenta exhibits a peak at the heavy resonance mass, regardless of the chosen MAOS scheme and the detailed mass spectrum of the particles in the cascade. We stress that the MAOS invariant mass can be used as a clean signal of new particle resonance produced at the Large Hadron Collider, as well as a model-independent method to measure the masses of new particles involved in the event.

DOI: 10.1103/PhysRevD.84.096001 PACS numbers: 11.80.Cr, 12.60.−i, 14.80.−j

I. INTRODUCTION

The naturalness principle predicts that there is new physics beyond the standard model (SM) at TeV scale, which is the scale of the Large Hadron Collider (LHC) experiment running now at CERN. It has also been claimed that one of the most important ingredients for the new physics model is the existence of a viable dark matter candidate, which is usually a weakly interacting massive particle (WIMP). In large classes of the new physics scenarios, the WIMP is often stabilized by a discrete parity, which consequently yields a generic collider signature with the missing particles always in pairs. Well-known examples such as supersymmetric (SUSY), little Higgs, and extra-dimensional models include a WIMP, which is the lightest new particle stabilized by a Z_2 parity [1–3]. The typical collider signature of the new physics model with conserved Z_2 parity is the production of a new particle pair, decaying to some visible SM particles (multiple leptons and/or jets) *plus* invisible WIMPs in the final state.

To uncover the underlying physics, one needs the information of the particle properties such as mass and spin, which can be revealed from the reconstruction of the signal events. However, in hadron colliders, it is generically impossible because the center-of-mass frame of the partonic collision is unknown and there are two invisible WIMPs in each event. Still, it has been proposed that the new particle masses might be determined by various kinematic variables such as the end points of the invariant mass distributions, transverse variables, and the techniques using the on-shell mass constraints in various new physics processes with the pair-produced new particles [4].

In this paper, we consider a new physics event,[1]

$$\begin{aligned} pp(\bar{p}) &\to X + U \to Y_1 Y_2 + U \\ &\to V_1(p)\chi_1(k)V_2(q)\chi_2(l) + U(u), \end{aligned} \tag{1}$$

where X, Y_i, and χ_i $(i = 1, 2)$ are new particles with *a priori* unknown mass, and U stands for visible particles not associated with the decay of X such as jets from the initial state radiation. We assume that X has even Z_2 parity, while Y_i and χ_i have odd Z_2 parity. Consequently, X can be resonantly produced and decay into a parity-odd particle pair. V_i's denote visible particles and χ_i's invisible ones, which yield the missing transverse momentum of the event,

$$\not{\mathbf{p}}_T = -\mathbf{p}_T - \mathbf{q}_T - \mathbf{u}_T = \mathbf{k}_T + \mathbf{l}_T. \tag{2}$$

A similar event topology has recently received a lot of attention. It describes the dilepton channel of the top-pair produced in the s-channel mediation of the color sextet bosons [6], or axigluon [7] at hadron colliders. In this case, the eight unknown components of two neutrino four-momenta can be solved from the six on-shell mass conditions on the top quarks, W bosons, and neutrinos in addition to the two constraints from the missing transverse momentum measurements, up to four possible solutions, as well as two combinations due to the charge ambiguity on b quarks [8]. In fact, the event topology (1) is one of the typical signatures of the new physics model with the WIMP stabilized by Z_2-parity, for instance, the heavy neutral SUSY Higgs boson (H/A) decaying to a pair of neutralinos ($\tilde{\chi}_i^0$) [9,10] or the $n = 2$ Kaluza-Klein (KK) Z boson ($Z^{(2)}$) decaying to a pair of $n = 1$ KK leptons ($l^{(1)}$) [11], producing the final state of several visible SM particles + WIMPs. The masses of the new particles involved in the decay chain are generically unknown, and the number of decays in the chain might be too short to constrain the unknown masses and invisible momenta in many new physics scenarios unlike the aforementioned top-pair process.

[1]The event topology is the same as the "antler" diagram, which was studied in [5]. However, here we assume that m_X is unknown *a priori*.

It has been claimed in the literature that it might be possible to measure the particle masses by constructing the transverse mass variables even if there are several invisible particles in the final state [12–14]. However, we note that the end-point position of the transverse mass distribution depends on the existence of kinematic configurations, which might be forbidden in some models. On the other hand, it has been recently found that the M_{T2}-assisted on-shell (MAOS) method [15], which was introduced to approximate the invisible particle momenta in the physics processes with conserved Z_2 parity, can be used to measure the SM Higgs boson mass in the dileptonic WW process [16]. We show that the MAOS method can be adopted to construct the invariant mass in the case of the event topology (1), thus enabling one to measure the resonance mass in a model-independent way.

This paper is organized as follows. In Sec. II, we discuss the features of the transverse mass variable for the full system, focusing on the behavior of its end point. Then, in Sec. III, we describe the definition and the types of solutions for the M_{T2} variable, which is an integral part of constructing the MAOS momenta, as well as known to be useful for measuring the masses of the intermediate on-shell states and the WIMP. For each type of the M_{T2} solution, the MAOS momenta have distinctive features, which lead to proposing various schemes of the MAOS reconstruction, as discussed in Sec. IV, where the construction of the invariant mass using the MAOS momenta is also described. The comparison between the MAOS schemes and the features of the MAOS invariant mass are shown by performing a Monte Carlo (MC) study in Sec. V. We summarize our conclusions in Sec. VI.

II. TRANSVERSE MASS OF THE FULL SYSTEM: M_T

In this section, we discuss some features of the transverse mass for the event topology (1). The impossibility of constructing the invariant mass of the decay system due to the existence of invisible particles in the final state leads to the proposal of a transverse mass variable, which does not use the unknown longitudinal component of the momenta [17]. The transverse mass for the event type (1) can be written as

$$M_T^2(Y_1Y_2) = m_{V_1V_2}^2 + m_{\chi_1\chi_2}^2 + 2(\sqrt{|\mathbf{p}_T^{V_1V_2}|^2 + m_{V_1V_2}^2} \times \sqrt{|\mathbf{p}_T^{\chi_1\chi_2}|^2 + m_{\chi_1\chi_2}^2} - \mathbf{p}_T^{V_1V_2}\cdot\mathbf{p}_T^{\chi_1\chi_2}), \quad (3)$$

where m_α and $\mathbf{p}_T^\alpha$ denote the invariant mass and the transverse momentum, respectively, of $\alpha = V_1V_2$, $\chi_1\chi_2$. It is then obvious that $M_T(Y_1Y_2)$ is bounded from above by m_X, thus making the determination of m_X possible if $M_T(Y_1Y_2)$ is correctly constructed event by event. It is, however, generally impossible to determine $m_{\chi_1\chi_2}$ event by event, even though the lower bound might be deduced from the knowledge of the event topology and m_{χ_i} values in some cases, e.g., the SM Higgs boson which decays into two leptonically decaying W bosons ($h \to WW \to l\nu l'\nu'$). If the lower bound of $m_{\chi_1\chi_2}$ is determined, it must be always true that

$$M_T(Y_1Y_2)|_{m_{\chi_1\chi_2}=m_{\chi_1\chi_2}^{\min}} \le M_T(Y_1Y_2)|_{m_{\chi_1\chi_2}=m_{\chi_1\chi_2}^{\text{true}}} \le m_X, \quad (4)$$

since $M_T(Y_1Y_2)$ is a monotonically increasing function of $m_{\chi_1\chi_2}$. This fact unties us from ignorance of the event-by-event values of $m_{\chi_1\chi_2}$, and consequently allows us to construct the transverse mass, which can be used to extract the information of m_X [12,13]. For the sake of discussion from now on, we focus on the symmetric decay chains, i.e. $m_{Y_1} = m_{Y_2} = m_Y$ and $m_{\chi_1} = m_{\chi_2} = m_\chi$. However, we notice that the arguments below can be generalized to the case of asymmetric decay chains.

If m_χ is unknown and there is no viable theoretical assumption on the lower bound of $m_{\chi\chi}$, the best choice will be

$$M_T^2(0) \equiv M_T^2(Y_1Y_2)|_{m_{\chi_1\chi_2}=0} = m_{V_1V_2}^2 + 2|\not{\mathbf{p}}_T|\sqrt{|\mathbf{p}_T + \mathbf{q}_T|^2 + m_{V_1V2}^2} - 2(\mathbf{p}_T + \mathbf{q}_T)\cdot\not{\mathbf{p}}_T, \quad (5)$$

then $M_T^{\max}(0) = m_X$ if and only if $m_{\chi_1\chi_2}^{\min} = 0$. The maximum of $M_T(0)$ occurs when χ_i's are moving parallel to each other in the X rest frame, and the invariant mass of the visible particles is minimized. Consequently, the analytic expression of the $M_T^{\max}(0)$ is obtained as [13]

$$M_T^{\max}(0) = \frac{m_X}{2m_Y^2}(\Lambda + \sqrt{\Lambda^2 - 4m_Y^2(m_V^{\min})^2}), \quad (6)$$

where $\Lambda \equiv m_Y^2 - m_\chi^2 + (m_V^{\min})^2$ and $m_V^{\min} \equiv \min\{m_{V_1}, m_{V_2}\}$ for all the events. If $m_V^{\min} = 0$,

$$M_T^{\max}(0) = m_X\left(1 - \frac{m_\chi^2}{m_Y^2}\right), \quad (7)$$

which shows that the $M_T(0)$ distribution can never reach m_X if χ_i is massive. The $M_T(0)$ variable was found to be useful for measuring the SM Higgs boson mass in dileptonic WW decay mode [12].

On the other hand, in many new physics scenarios, m_χ is likely to be determined by the other kinematic variables such as the M_{T2} kink, which will be described in Sec. III, or possibly the combinations of the invariant mass end points from various other decay processes. In such cases, the more plausible choice of the $m_{\chi_1\chi_2}^{\min}$ value will be $2m_\chi(= m_{\chi_1} + m_{\chi_2})$ as

$$M_T^2(2m_\chi) = m_{V_1V_2}^2 + 4m_\chi^2 + 2\sqrt{|\mathbf{p}_T + \mathbf{q}_T|^2 + m_{V_1V_2}^2}\sqrt{|\not{\mathbf{p}}_T|^2 + 4m_\chi^2} - 2(\mathbf{p}_T + \mathbf{q}_T)\cdot\not{\mathbf{p}}_T. \quad (8)$$

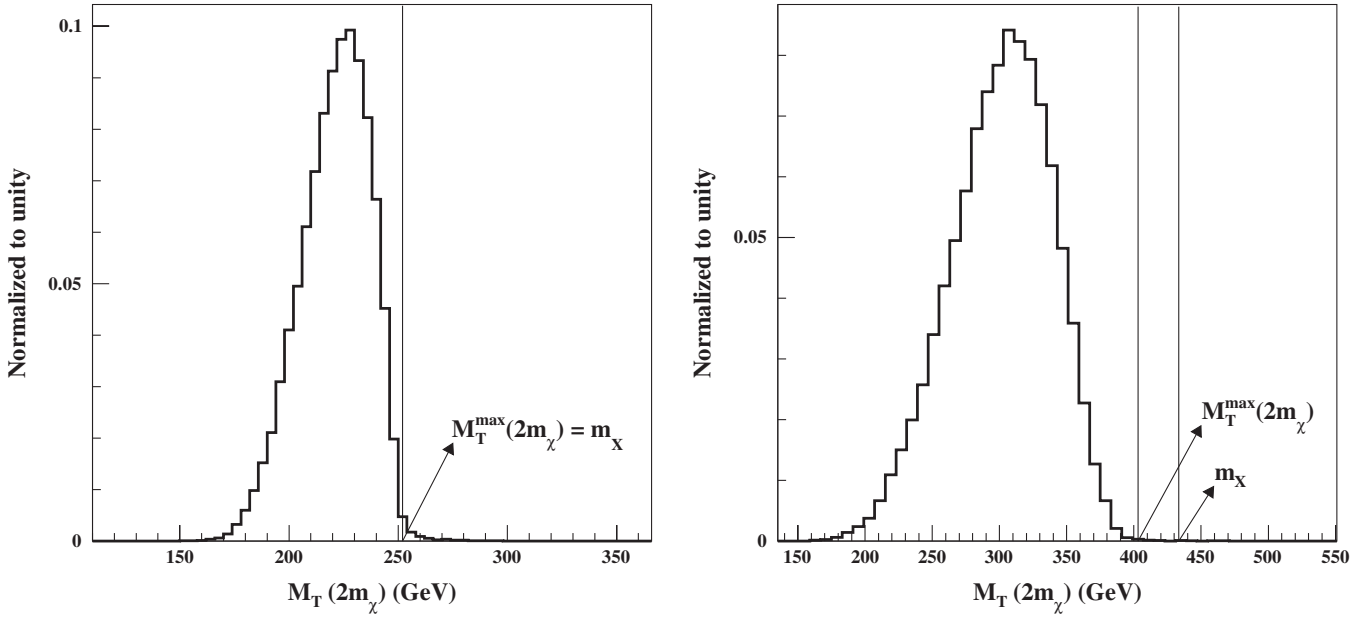

FIG. 1. Comparison plot of the $M_T(2m_\chi)$ distributions of the SUSY process $H/A \to \tilde{\chi}_2^0\tilde{\chi}_2^0 \to l^+l^-\tilde{\chi}_1^0 l^+l^-\tilde{\chi}_1^0$. The mass parameters are $(m_{\tilde{\chi}_2^0}, m_{\tilde{\chi}_1^0}) \simeq (110, 61)$ GeV for both plots, and $m_{H/A} = 252(433)$ GeV for the left (right) panel. See Sec. V for a detailed description of the model and its simulation.

But still, the knowledge of m_χ does not guarantee the saturation of the bound on m_X. If there is no kinematic configuration in which $m_{\chi_1\chi_2} = 2m_\chi$ is achieved, the $M_T(2m_\chi)$ distribution will not reach m_X, because

$$M_T(Y_1Y_2)|_{m_{\chi\chi}=2m_\chi} < M_T(Y_1Y_2)|_{m_{\chi\chi}=m_{\chi\chi}^{\min}} \le M_T(Y_1Y_2)|_{m_{\chi\chi}=m_{\chi\chi}^{\text{true}}} \le m_X. \quad (9)$$

The condition for the existence of the kinematic configuration saturating the bound of $M_T(2m_\chi)$ up to m_X depends on the mass pattern of the involved particles in the decay channel, and has been derived in [13]

$$m_X \le \frac{m_Y^2 + m_\chi^2 - (m_V^{\min})^2}{m_\chi}. \quad (10)$$

One can see that it may be impossible to satisfy the above condition if X is too heavy, compared with the mass scale of its decay products. In case the condition (10) is not satisfied, m_X is above the upper bound of $M_T(2m_\chi)$, which depends on the possible range of $m_{V_1V_2}$,

$$M_T^{\max}(2m_\chi) = 2m_\chi + m_{V_1V_2}^{\max} = 2m_\chi + \frac{m_X}{2m_Y^2} \times \left(\Lambda + \sqrt{1 - \frac{4m_Y^2}{m_X^2}}\sqrt{\Lambda^2 - 4m_Y^2(m_V^{\min})^2}\right). \quad (11)$$

In order to check the properties of $M_T(2m_\chi)$ discussed above, we have generated MC event samples of heavy neutral Higgs bosons (H/A) for two SUSY benchmark points. In this model, the heavy Higgs boson decays to a pair of next-to-lightest neutralinos ($\tilde{\chi}_2^0$), producing the final state of four charged leptons and a lightest neutralino ($\tilde{\chi}_1^0$) pair via a three-body process, $\tilde{\chi}_2^0 \to l^+l^-\tilde{\chi}_1^0$. The detailed description of the chosen model is given in Sec. V. In Fig. 1, we exhibit the $M_T(2m_\chi)$ distribution for benchmark points with relatively light (left panel) and heavy (right panel) H/A. One finds that the condition (10) is satisfied in the case of a relatively light H/A scenario, such that the $M_T^{\max}(2m_\chi)$ corresponds to $m_{H/A}$. However, it is not satisfied in the heavy H/A case, thus $M_T^{\max}(2m_\chi)$ is lower than $m_{H/A}$. This observation shows that the M_T method depends highly on the underlying model, i.e. the mass splitting of the on-shell states involved in the event. Hence, one needs accurate knowledge of m_Y and possibly the range of m_V as well as m_χ to determine m_X.

III. ALTERNATIVE TRANSVERSE MASS: M_{T2}

In a situation where there are two invisible particles in the event, one may exploit the event variable M_{T2}, which was proposed to measure the particle masses in an event topology such as $Y_1Y_2 \to V_1(p)\chi_1(k)V_2(q)\chi_2(l)$, which is, for instance, the typical collider event of pair-produced SUSY particles [18]. Not only is the M_{T2} useful for measuring the new particle masses even in the event topology (1), but it is also an integral part of the definition of the MAOS momenta, which will be described in the next section. M_{T2} can also be defined in the asymmetric decay event with $m_{Y_1} \neq m_{Y_2}$ and $m_{\chi_1} \neq m_{\chi_2}$ [19]. However, here we consider only the event type with the symmetric decay

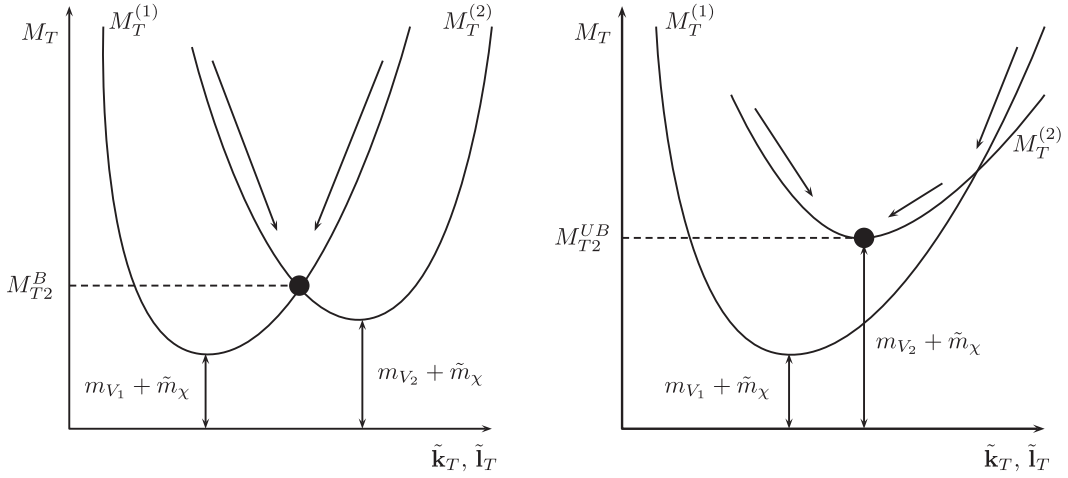

FIG. 2. A schematic picture of the balanced (left panel) and the unbalanced (right panel) M_{T2} solutions.

chains as in the previous section. The M_{T2} variable is defined as

$$M_{T2} \equiv \min_{\tilde{\mathbf{k}}_T+\tilde{\mathbf{l}}_T=\not{\mathbf{p}}_T} [\max\{M_T^{(1)}(\mathbf{p}_T, \tilde{\mathbf{k}}_T, \tilde{m}_\chi), M_T^{(2)}(\mathbf{q}_T, \tilde{\mathbf{l}}_T, \tilde{m}_\chi)\}], \tag{12}$$

where $M_T^{(1)}$ and $M_T^{(2)}$ are the transverse masses of the Y_1 and Y_2 systems, respectively,

$$\begin{aligned}(M_T^{(1)})^2 &= m_{V_1}^2 + \tilde{m}_\chi^2 + 2\sqrt{|\mathbf{p}_T|^2 + m_{V_1}^2}\sqrt{|\tilde{\mathbf{k}}_T|^2 + \tilde{m}_\chi^2} \\ &\quad - 2\mathbf{p}_T \cdot \tilde{\mathbf{k}}_T, \\ (M_T^{(2)})^2 &= m_{V_2}^2 + \tilde{m}_\chi^2 + 2\sqrt{|\mathbf{q}_T|^2 + m_{V_2}^2}\sqrt{|\tilde{\mathbf{l}}_T|^2 + \tilde{m}_\chi^2} \\ &\quad - 2\mathbf{q}_T \cdot \tilde{\mathbf{l}}_T. \end{aligned} \tag{13}$$

Here, $\tilde{m}_\chi$, $\tilde{\mathbf{k}}_T$, and $\tilde{\mathbf{l}}_T$ are input trial values of the mass and transverse momenta of the invisible particles. They are *hypothesized* values that parametrize our ignorance of the allocation of missing transverse momenta into the invisible particle momenta in each event, in addition to the true value of m_χ. The momentum constraint in the minimization automatically guarantees that the sum of the hypothesized momenta is equal to that of the true momenta, which can be determined event by event. When the input trial mass $\tilde{m}_\chi$ equal the true mass m_χ,

$$M_{T2}^{\max}(\tilde{m}_\chi = m_\chi) = m_Y, \tag{14}$$

provided that the parent particles Y_i are on shell.

The M_{T2} solution for the hypothesized momenta can be classified into two configurations, *unbalanced* and *balanced*. The value of M_{T2} is given by $M_T^{(1)} = M_T^{(2)}$ in the balanced configuration, while the unbalanced M_{T2} solution is achieved when the condition for the balanced configuration, which will be shown shortly, is not valid. The type of the M_{T2} solution can be deduced from the value of $M_T^{(i)}$ at the hypothesized momenta which give the global minimum of $M_T^{(j)}$ $(i \neq j)$. The global minimum of $M_T^{(1)}$ $(M_T^{(2)})$ corresponds to the stationary point for given values of m_{V_1} (m_{V_2}) and $\tilde{m}_\chi$,

$$(M_T^{(1)})_{\min} = m_{V_1} + \tilde{m}_\chi, \quad (M_T^{(2)})_{\min} = m_{V_2} + \tilde{m}_\chi, \tag{15}$$

when $\tilde{\mathbf{k}}_T = (\tilde{m}_\chi/m_{V_1})\mathbf{p}_T$ and $\tilde{\mathbf{l}}_T = (\tilde{m}_\chi/m_{V_2})\mathbf{q}_T$, respectively. The M_{T2} value of the event will be obtained from the balanced configuration when

$$M_T^{(i)} \geq (M_T^{(j)})_{\min} \quad (i \neq j) \tag{16}$$

is satisfied at the stationary points. [See the left panel of Fig. 2 for illustration.] For events in which the condition (16) is not satisfied, the M_{T2} is given by the larger value between global minima of $M_T^{(i)}$ at the stationary points,

$$\begin{aligned} M_{T2}^{UB} &= \max\{(M_T^{(1)})_{\min}, (M_T^{(2)})_{\min}\} \\ &= \begin{cases} m_{V_1} + \tilde{m}_\chi & \text{if } M_T^{(1)} > M_T^{(2)}, \\ m_{V_2} + \tilde{m}_\chi & \text{if } M_T^{(1)} < M_T^{(2)}. \end{cases} \end{aligned} \tag{17}$$

On the other hand, the solution for the balanced configuration needs some nontrivial consideration. The analytic expression of M_{T2} was first derived in [20], then further simplified in [21], by considering the event types with vanishing upstream transverse momentum (UTM), i.e. $\mathbf{u}_T = 0$ in (2).[2] It is given by

[2]Recently, the analytic expression of M_{T2} has been derived for some special kinematic configurations. See Ref. [22].

$$(M_{T2}^{B})^2 = (M_T^{(1)})^2 = (M_T^{(2)})^2 = \tilde{m}_\chi^2 + A_T + \sqrt{\left(1 + \frac{4\tilde{m}_\chi^2}{2A_T - m_{V_1}^2 - m_{V_2}^2}\right)(A_T^2 - m_{V_1}^2 m_{V_2}^2)}, \tag{18}$$

where

$$A_T \equiv \sqrt{|\mathbf{p}_T|^2 + m_{V_1}^2}\sqrt{|\mathbf{q}_T|^2 + m_{V_2}^2} + \mathbf{p}_T \cdot \mathbf{q}_T, \tag{19}$$

which is invariant under the back-to-back transverse boost. This quantity is closely related to the M_{CT} in [23], which has been further generalized to the M_{CT2} in the case of two invisible particles in the event [24].

The investigation of the M_{T2} from the above expressions showed that the end-point position of the M_{T2} distribution, $M_{T2}^{\max}$, as a function of the $\tilde{m}_\chi$ has a kink structure at $\tilde{m}_\chi = m_\chi$ if the invariant mass of the visible particles is not fixed, but has a certain range in each decay chain [21]. It was also noticed that the kink structure of $M_{T2}^{\max}(\tilde{m}_\chi)$ will appear when there is a sizable amount of UTM in the events [25]. The M_{T2}-kink method makes it possible to measure m_χ and m_Y simultaneously even if the decay chain is not long enough to constrain all the unknowns in the event. This observation suggests that the M_{T2}-kink method might also be very useful to measure m_Y and m_χ in the event topology (1), specifically, if V_i is a set of more than two visible particles and/or the full system of Y_1Y_2 is boosted by the UTM.

If $\tilde{m}_\chi = m_{V_1} = m_{V_2} = 0$, Eq. (18) becomes even simpler as

$$(M_{T2})^2|_{\tilde{m}_\chi=0} = 2A_T = 2(|\mathbf{p}_T||\mathbf{q}_T| + \mathbf{p}_T \cdot \mathbf{q}_T). \tag{20}$$

Interestingly, the authors of [16] have recently claimed that the M_{T2} method can be applied to measure the mass of the SM Higgs boson in dileptonic WW mode, which is also the event type (1), and used as an event selection cut to efficiently suppress the background processes.

IV. CONSTRUCTION OF THE INVARIANT MASS USING MAOS MOMENTA

After discussing the transverse mass variables, we deal with the construction method of the invariant mass. In Ref. [15], the authors introduced a systematic approximation to the invisible momenta by combining the M_{T2} solution with the on-shell relations for generic events like $Y_1Y_2 \to V_1(p)\chi_1(k)V_2(q)\chi_2(l)$. The MAOS momenta was originally proposed to determine the spin of new particles produced at hadron colliders [15,26,27], but it was later realized that it might also be very useful for the mass measurement [16,28].

The definition of MAOS momenta is composed of two parts, the transverse and the longitudinal components. The transverse components of the invisible momenta are set by the trial momenta which give the value of M_{T2},

$$\mathbf{k}_T^{\text{maos}} = \tilde{\mathbf{k}}_T, \qquad \mathbf{l}_T^{\text{maos}} = \tilde{\mathbf{l}}_T, \tag{21}$$

where $\tilde{\mathbf{k}}_T$ and $\tilde{\mathbf{l}}_T$ are determined once we minimize $\max\{M_T^{(1)}, M_T^{(2)}\}$ in (12), among all possible trial $\tilde{\mathbf{k}}_T$ and $\tilde{\mathbf{l}}_T$ satisfying $\tilde{\mathbf{k}}_T + \tilde{\mathbf{l}}_T = \not{\mathbf{p}}_T$. The longitudinal and energy components are then calculated by the on-shell relations for both χ_i and Y_i,

$$(k^{\text{maos}})^2 = \tilde{m}_{\chi_1}^2, \qquad (l^{\text{maos}})^2 = \tilde{m}_{\chi_2}^2, \tag{22}$$

$$(p + k^{\text{maos}})^2 = \tilde{m}_{Y_1}^2, \qquad (q + l^{\text{maos}})^2 = \tilde{m}_{Y_2}^2, \tag{23}$$

where $\tilde{m}_{\chi_i}$ and $\tilde{m}_{Y_i}$ $(i = 1, 2)$ are input trial masses of the invisible and the parent particles, respectively. The longitudinal components of the MAOS momenta are then given by

$$k_L^{\text{maos}} = \frac{1}{E_T^2(p)}[\mathcal{A}\, p_L \pm \sqrt{p_L^2 + E_T^2(p)}\sqrt{\mathcal{A}^2 - E_T^2(p)E_T^2(k)}],$$
$$l_L^{\text{maos}} = \frac{1}{E_T^2(q)}[\mathcal{B} q_L \pm \sqrt{q_L^2 + E_T^2(q)}\sqrt{\mathcal{B}^2 - E_T^2(q)E_T^2(l)}], \tag{24}$$

where

$$\mathcal{A} = \frac{1}{2}(\tilde{m}_{Y_1}^2 - \tilde{m}_{\chi_1}^2 - m_{V_1}^2) + \mathbf{p}_T \cdot \mathbf{k}_T^{\text{maos}},$$
$$\mathcal{B} = \frac{1}{2}(\tilde{m}_{Y_2}^2 - \tilde{m}_{\chi_2}^2 - m_{V_2}^2) + \mathbf{q}_T \cdot \mathbf{l}_T^{\text{maos}},$$
$$E_T(p) = \sqrt{|\mathbf{p}_T|^2 + m_{V_1}^2},$$
$$E_T(q) = \sqrt{|\mathbf{q}_T|^2 + m_{V_2}^2}, \tag{25}$$
$$E_T(k) = \sqrt{|\mathbf{k}_T^{\text{maos}}|^2 + \tilde{m}_{\chi_1}^2},$$
$$E_T(l) = \sqrt{|\mathbf{l}_T^{\text{maos}}|^2 + \tilde{m}_{\chi_2}^2}.$$

From the above expressions, it is obvious that both k_L^{maos} and l_L^{maos} are real if and only if

$$|\mathcal{A}| \geq E_T(p)E_T(k), \qquad |\mathcal{B}| \geq E_T(q)E_T(l),$$

or equivalently

$$\tilde{m}_{Y_1} \geq M_T^{(1)}, \qquad \tilde{m}_{Y_2} \geq M_T^{(2)}, \tag{26}$$

where $M_T^{(1)}$ and $M_T^{(2)}$ are the transverse masses defined in (13) for $\tilde{\mathbf{k}}_T = \mathbf{k}_T^{\text{maos}}$, $\tilde{\mathbf{l}}_T = \mathbf{l}_T^{\text{maos}}$, and the trial masses $\tilde{m}_{\chi_i}$. If the decay chain is symmetric, i.e. $\tilde{m}_{\chi_1} = \tilde{m}_{\chi_2} = \tilde{m}_\chi$ and $\tilde{m}_{Y_1} = \tilde{m}_{Y_2} = \tilde{m}_Y$, the above condition reduces to

$$\tilde{m}_Y \geq \max\{M_T^{(1)}, M_T^{(2)}\}, \tag{27}$$

so that the MAOS momenta are always real if the value of $M_{T2}^{\max}(\tilde{m}_\chi)$ is chosen as the trial mass of the parent particle

for a given $\tilde{m}_\chi$. Note that the true mass values m_Y and m_χ automatically satisfy the condition (27) because $M_{T2}^{\max}(\tilde{m}_\chi = m_\chi) = m_Y$. For the end-point events of the balanced M_{T2}, one has $M_T^{(1)} = M_T^{(2)} = \tilde{m}_Y$, and thus $k^{\rm maos}$ and $l^{\rm maos}$ correspond to the unique solution of the constraints (2), (22), and (23). In this case, since the true invisible momenta also satisfy the same conditions, they must be equal to the unique solution when the true mass values m_χ and m_Y are inserted in Eqs. (22) and (23),

$$k^{\rm maos} = k^{\rm true}, \qquad l^{\rm maos} = l^{\rm true}. \tag{28}$$

On the other hand, this is not true for the end-point events of the unbalanced M_{T2} because $M_T^{(1)} \neq M_T^{(2)}$, which means that only one side of the MAOS momenta corresponds to the true invisible momenta. This argument indicates that the accuracy of the MAOS momenta can be controlled by imposing a suitable M_{T2} cut, which selects the subset of events near the M_{T2} end point. Even if m_χ or m_Y were poorly measured, it was shown that the MAOS momenta would provide a good approximation to the true invisible momenta by setting $\tilde{m}_\chi = 0$ and $\tilde{m}_Y = M_{T2}^{\max}(\tilde{m}_\chi = 0)$ [15]. One inevitable problem in this definition is that there is generically a four-fold ambiguity on the longitudinal and energy components as can be seen in Eqs. (24). In the absence of any extra constraints or viable assumptions on the kinematic structure of the event, it is clear that there should be no preference of one solution to the others. We label this scheme of obtaining the solution of the invisible momenta as the first kind of MAOS or MAOS1 to distinguish it from the other schemes in what follows.

In addition to the ambiguity of the solutions, a serious problem will arise when one or both parent particles Y_i are off shell. The on-shell conditions (23) can be adopted only if the parent particles are on shell, such that the mass values are fixed for all the events. To make the MAOS method applicable to the situation where the on-shell conditions are not valid, one may consider modifying the on-shell relations. One possible scheme is to substitute the event variable M_{T2}, instead of the fixed value $\tilde{m}_Y$, by

$$(p + k^{\rm maos})^2 = M_{T2}^2, \qquad (q + l^{\rm maos})^2 = M_{T2}^2. \tag{29}$$

Then, for the events of the balanced M_{T2}, one has $M_T^{(1)} = M_T^{(2)} = M_{T2}$, and thus $k_L^{\rm maos}$ and $l_L^{\rm maos}$ become unique (MAOS2). This is the scheme which was used to measure the SM Higgs boson mass in [16], for both $m_h \geq 2m_W$ and $m_h < 2m_W$ cases.[3] On the other hand, for the events of the unbalanced M_{T2}, i.e. $M_T^{(1)} \neq M_T^{(2)}$, a two-fold ambiguity still remains on one side of the longitudinal components.

The only possible way to obtain the unique solution of the longitudinal and energy components for all the events is to take

$$(p + k^{\rm maos})^2 = (M_T^{(1)})^2, \qquad (q + l^{\rm maos})^2 = (M_T^{(2)})^2. \tag{30}$$

Adopting the above new scheme, the longitudinal components are given by

$$k_L^{\rm maos} = \frac{E_T(k)}{E_T(p)} p_L, \qquad l_L^{\rm moas} = \frac{E_T(l)}{E_T(q)} q_L, \tag{31}$$

which are uniquely defined in the events for both balanced and unbalanced M_{T2} (MAOS3). Note that if the true mass m_χ is chosen as the input, the MAOS momenta will be equal to the true invisible momenta for the end-point events of the balanced M_{T2} because $M_T^{(1)} = M_T^{(2)} = M_{T2}^{\max}(m_\chi) = m_Y$ corresponds to the true parent particle mass. Although it is not true for the events of the unbalanced M_{T2}, one side of the MAOS momenta ($k^{\rm maos}$ if $M_T^{(1)} = M_{T2}^{\max} = m_Y > M_T^{(2)}$) still gives the true momenta if the end-point events of M_{T2} were selected. Accordingly, one finds that the accuracy of the MAOS momenta can be still controlled by the M_{T2} cut, which might also be useful for suppressing the SM backgrounds in the search for a new physics signal at the LHC [29].

Applying the MAOS method to the event topology (1), it is possible to construct the invariant mass of the $Y_1 Y_2$ system,

$$(p + q + k^{\rm maos} + l^{\rm maos})^2 \equiv (m_X^{\rm maos})^2. \tag{32}$$

Then, the successful reconstruction of the invisible momenta by the MAOS method ensures that the MAOS invariant mass ($m_X^{\rm maos}$) distribution has a peak at the true mass m_X, which will also be confirmed by the numerical simulation in the next section. The distinctive feature of the MAOS method is that it is less model dependent than transverse mass variables since the latter highly depends on the mass gaps in the model. Even when the resonance particle X is too heavy, the peak position of the MAOS invariant mass distribution corresponds to m_X, which might be beyond the transverse mass distribution. The requisites for constructing the MAOS invariant mass are the assumption of the event topology (1) and the knowledge of m_χ, which are also essential for constructing $M_T(2m_\chi)$ in Sec. II. We also note that the MAOS invariant mass is distinguished by the peak structure, and it is generally less vulnerable to the background and momentum smearing effects. The clear peak structure of the MAOS invariant mass can be viewed as the smoking-gun signal of the heavy resonance produced at hadron colliders.

V. MONTE CARLO STUDY: HEAVY SUSY HIGGS BOSONS

In this section, we illustrate the discussion of the previous section by performing a MC study for the decay signal of heavy SUSY Higgs bosons H/A into a pair of next-to-lightest neutralino, $\tilde{\chi}_2^0$, followed by the decay

[3]Note that there is only balanced configuration for the SM Higgs decay events, $h \to WW \to l\nu l'\nu'$.

$\tilde{\chi}_2^0 \to l^+ l^- \tilde{\chi}_1^0$ ($l = e, \mu$). This process results in a four-lepton plus missing transverse energy final state,

$$H/A \to \tilde{\chi}_2^0 \tilde{\chi}_2^0 \to l^+ l^- l^+ l^- + \not{E}_T. \tag{33}$$

As a specific example, we examined two benchmark points in the minimal supergravity scenario chosen in [10]. The superparticle mass spectrum has been calculated with SOFTSUSY [30], and is given by

(i) point A: $m_{H/A} = 252$ GeV, $m_{\tilde{\chi}_2^0} = 110$ GeV, $m_{\tilde{\chi}_1^0} = 61$ GeV; and
(ii) point B: $m_{H/A} = 433$ GeV, $m_{\tilde{\chi}_2^0} = 112$ GeV, $m_{\tilde{\chi}_1^0} = 62$ GeV.

We used PYTHIA 6.4 to generate the MC events in the LHC beam condition with the proton-proton center-of-mass energy of 14 TeV [31]. For the simple illustrative study, we have not considered the detector effects such as the momentum smearing effect and the identification efficiency of the leptons. The integrated luminosity is assumed to be large enough to measure the particle spectra. The main background process from the SM will be ZZ^*/γ^* with four leptons in the final state. This can be eliminated by requiring large missing energy and imposing a Z-veto cut, which rejects events of a dilepton pair with the invariant mass near m_Z. The dominant source of the background in the SUSY process is the production of leptons from the decays of neutralinos and charginos, produced by squarks and gluinos. In this case, however, the leptons are produced in association with jets, so that a jet-veto cut should be imposed to suppress this type of background. The direct production of a neutralino pair via the Drell-Yan processes could be challenging because it has the same final state. See Ref. [10] and Chap. 11 of [32] for a detailed study of the signature including the backgrounds at detector level. Here, we do not consider the background effect and the event selection cuts except the M_{T2} cut.

In the above benchmark points, $\tilde{\chi}_2^0$ decays to $\tilde{\chi}_1^0$ and two charged leptons via three-body process with an off-shell intermediate Z boson or slepton ($m_{\tilde{l}_R} = 141$ and 406 GeV for points A and B, respectively), such that $0 \le m_{l^+l^-} \le m_{\tilde{\chi}_2^0} - m_{\tilde{\chi}_1^0}$. The main difference between the benchmark points is the mass of H/A, which is relatively light in point A and heavier in point B. One can easily find that the condition (10) is not satisfied in point B, whereas it is satisfied in point A. This results in the position of $M_T^{\max}(2m_\chi)$ being lower than $m_{H/A}$, as can be seen in the right panel of Fig. 1.

To see the characteristic feature of the MAOS momenta, in Fig. 3 we show the difference between the reconstructed and the true momenta of $\tilde{\chi}_1^0$ for point A. The left panel includes the distributions of the full event set for the process (33) generated at the LHC condition, while the right panel shows the distributions of the top 10% subset events near the end point of M_{T2}. By definition, each MAOS scheme gives the same transverse MAOS momenta. For $k_L^{\text{maos}} - k_L^{\text{true}}$ in the MAOS1 and MAOS2 schemes, we construct their distributions using all the possible solutions

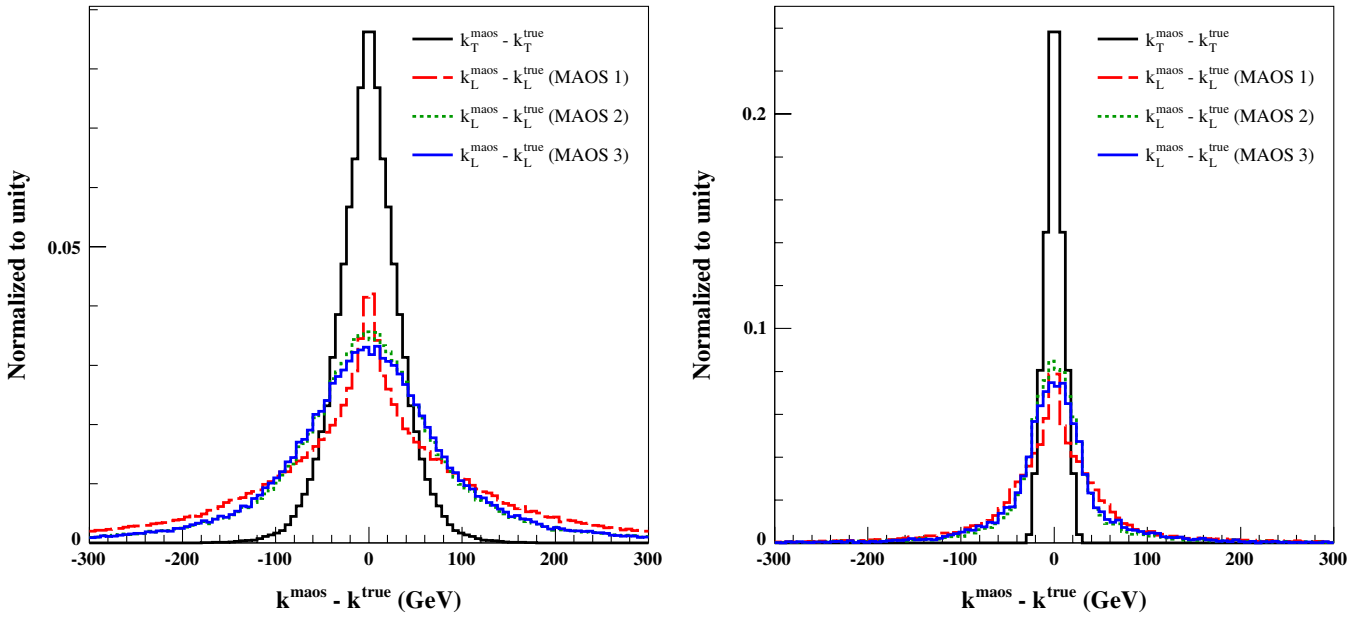

FIG. 3 (color online). The distributions of $\mathbf{k}_T^{\text{maos}} - \mathbf{k}_T^{\text{true}}$ and $k_L^{\text{maos}} - k_L^{\text{true}}$ for the full event set (left panel), and top 10% end-point events of M_{T2} (right panel) with the input mass $\tilde{m}_\chi = m_{\tilde{\chi}_1^0}$ for the model point A. For the MAOS1 scheme, the input mass for the parent particle $\tilde{m}_Y$ is set to $m_{\tilde{\chi}_2^0}$.

in each event. The result shows that the MAOS1 scheme is slightly better than the others if one considers the full event set. However, all the schemes provide a similar performance if one employs a suitable M_{T2} cut. This observation and the fact that the MAOS1 scheme cannot be adopted when one or both parent particles are off shell suggest that the MAOS2 or MAOS3 schemes can be used safely without a big loss of efficiency and regardless of whether the parent particles are on shell or not. The efficiency of the MAOS momenta will also vary as the detail of the matter content and the decay process in the model. It depends not only on the mass spectrum, but also on the coupling structure of the particles involved in the cascade decay. The mass gap of the decaying particles typically affects the size of the momentum of the visible particles, and their particular momentum direction might be forbidden by the helicity correlations. These consequently give rise to the different shape of the M_{T2} distribution, i.e., how populous are the events near the end point. In any case, as pointed out in the previous section, the accuracy of the MAOS momenta can be controlled by the M_{T2} cut. Although the study of the detailed model dependence regarding the efficiency of the MAOS reconstruction is beyond our scope here, we stress that it is worthwhile to study before the application to the experiments.

Next, we proceed to construct the invariant mass of H/A using the MAOS momenta following Eq. (32). In Fig. 4, we show the MAOS invariant mass distributions for the full event set with the input trial mass $\tilde{m}_\chi = m_{\tilde{\chi}_1^0}$ while varying the MAOS scheme. One can see that all the schemes provide a clear peak structure around $m_{H/A}$. This result again indicates that the performance of the MAOS momenta does not depend much on the adopted scheme. Figure 5 shows the dependency of the MAOS invariant mass on the input trial mass of the invisible particle. Although all the distributions have a peak structure for an arbitrary choice of the input trial mass, the peak is located at the true resonance mass, $m_{H/A}$, only when $\tilde{m}_\chi = m_{\tilde{\chi}_1^0}$ is chosen. In the right panels of Fig. 5, the top 30% near-end-point events of M_{T2} are used. This shows that the peak structure of the distributions is very clear for the subset of the events, while not changing the position of the peak. Our simulation proves that this feature does not depend on the MAOS scheme.

In real situations, one should consider the combinatorial uncertainty regarding the assignment of the visible particles to each chain. For points A and B, the assignment is uniquely determined if the event includes two different pairs of opposite-sign same-flavor leptons. On the other hand, there are two possible combinations when the event includes four leptons with the same flavor, i.e. $e^+e^-e^+e^-/\mu^+\mu^-\mu^+\mu^-$. One may select only the former type of events to reconstruct the invisible momenta while sacrificing the statistics. In a well-known model like the SM, one may calculate the likelihood functions of kinematic variables based on the model expectations, then select the combination which gives the most likely solution [33]. The other straightforward method is to use the value

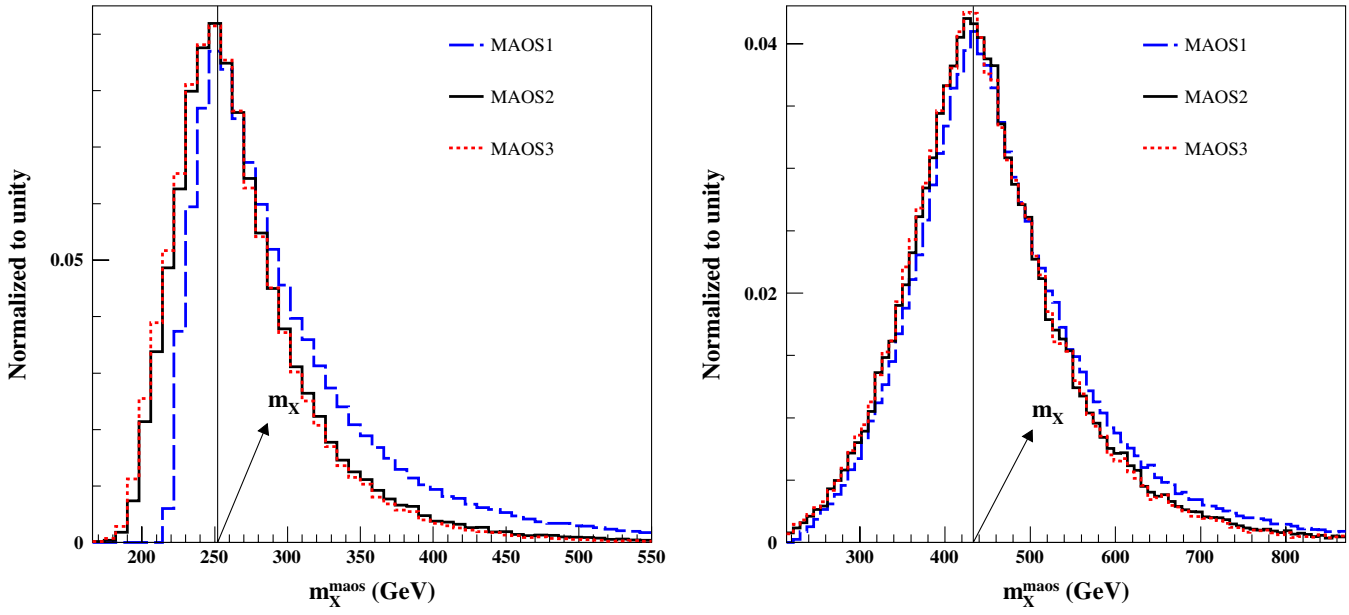

FIG. 4 (color online). The distributions of the MAOS invariant mass without the M_{T2} cut for point A (left panel) and point B (right panel) with the input mass $\tilde{m}_\chi = m_{\tilde{\chi}_1^0}$. In each panel, the MAOS1 (blue dashed), MAOS2 (black solid), and MAOS3 (red dotted) schemes are adopted to obtain the solution of the invisible momenta. For the MAOS1 scheme, the input mass for the parent particle mass $\tilde{m}_Y$ is set to $m_{\tilde{\chi}_2^0}$.

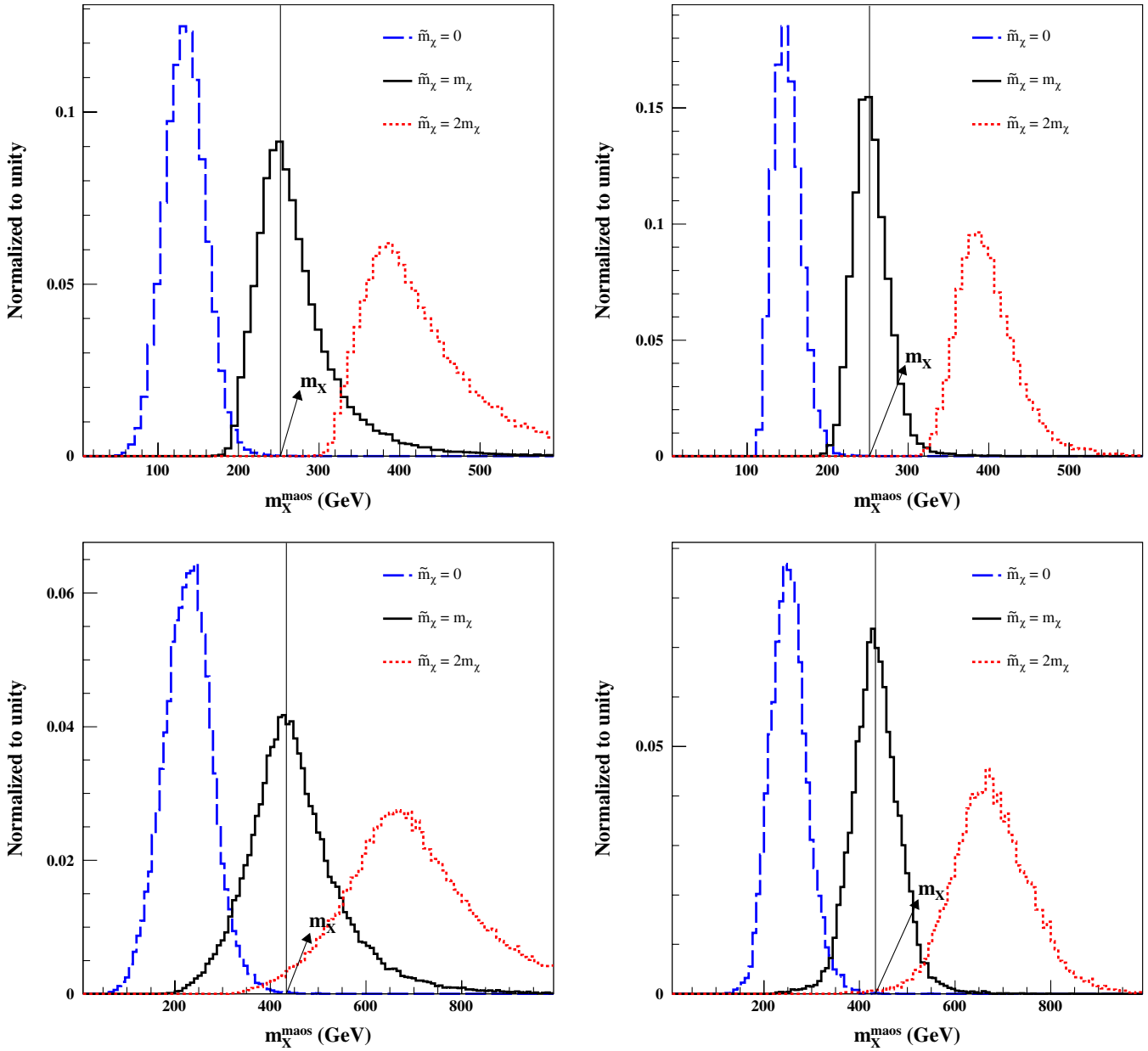

FIG. 5 (color online). The distributions of the MAOS invariant mass for point A (upper panels) and point B (lower panels). The full event set is used in the left frames, while the top 30% near-end-point events of M_{T2} are used in the right frames. The MAOS3 scheme is adopted to obtain the solution of invisible momenta.

of M_{T2} in the event, as done in [6,34]. For a given event, one can construct the M_{T2} of all possible combinations, then select the combination which gives the smallest value of the M_{T2}. It is actually the same as the $M_{T\mathrm{Gen}}$ defined in [20]. This method can be adopted because the M_{T2} from the correct pair will have the end point that is definitely related to the mass spectrum of the involved particles, whereas there is no such structure in the M_{T2} from the wrong pair, which results in a broad distribution in general. Our MC study shows that the method is useful for both points A and B. It selects the correct combination with 68% and 97% efficiency for points A and B, respectively. The different level of efficiency is caused by the fact that the decay products are relatively energetic in point B because of heavier H/A, and thus it makes the M_{T2} distribution of the wrong pair even broader. In Fig. 6, we present the MAOS invariant mass for the true combination (black solid), and the combination of four leptons with the smallest value of M_{T2} (red dotted). If there is only one combination, i.e. $e^+e^-\mu^+\mu^-$ in the event, we use the

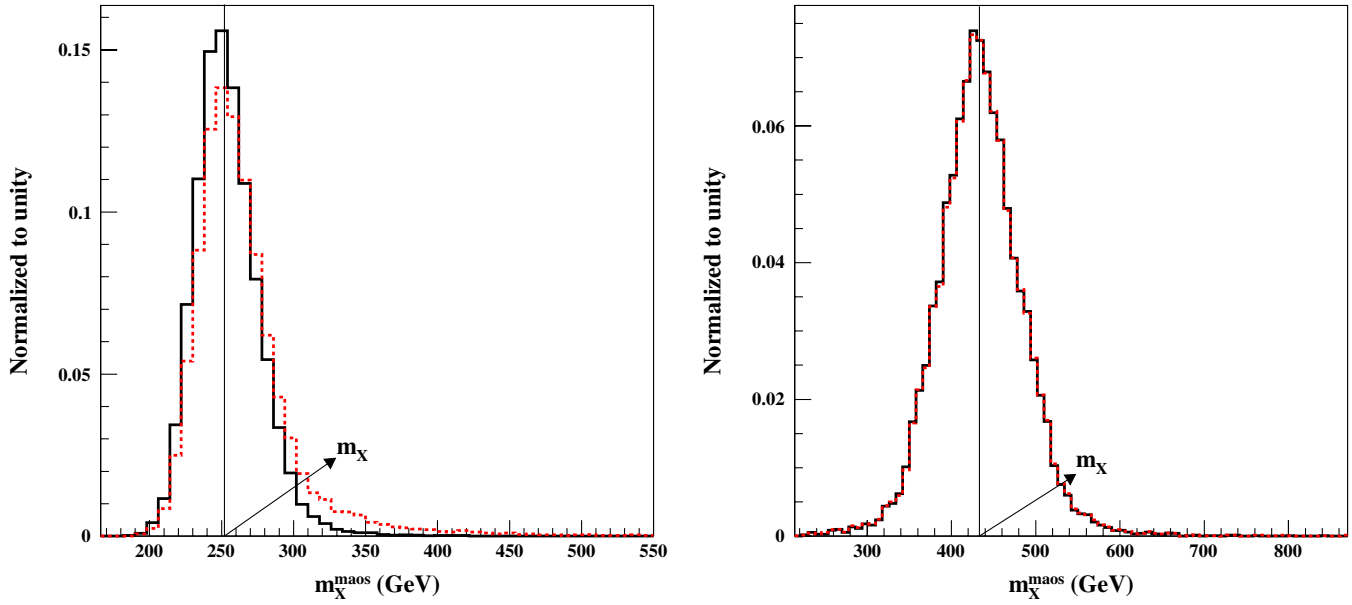

FIG. 6 (color online). The distributions of the MAOS invariant mass for point A (left panel) and point B (right panel) with the top 30% near-end-point events of M_{T2}. The MAOS3 scheme is adopted to construct the invariant masses, and the input trial mass $\tilde{m}_\chi$ is set to $m_{\tilde{\chi}_1^0}$. In each panel, the true combination of four leptons is used for the black solid distribution, while the combination with the smallest value of M_{T2} is used for the red dotted distribution.

combination in the MAOS reconstruction. The result shows that the overall structure of the distributions remains unchanged for both points A and B, such that the method of finding the correct pair using M_{T2} is successful.

VI. CONCLUSIONS

In this paper, we have examined the possibility of measuring the heavy resonance mass by constructing the invariant mass using the MAOS momenta. Regarding the MAOS reconstruction, we found that various schemes can be defined in order to obtain the MAOS momenta, in particular, the longitudinal and the energy components. The MAOS schemes are classified by the on-shell equations as summarized in Table I. Although the MAOS schemes provide different solutions in general, a similar level of efficiency can be obtained in the subset of the events near the end point of M_{T2}. We also note that the MAOS1 scheme is not applicable when one or both parent particles Y_i are off shell, whereas the MAOS2 and MAOS3 schemes do not have such a limitation. Using the MAOS reconstruction of the invisible momenta, one can construct the invariant mass of the full system. We have shown that the peak position of the MAOS invariant mass distribution always corresponds to the resonance mass, at which the end point of the transverse mass distribution may fail to point. This feature may enable one to deduce directly the mass scale of the heavy resonance even in the stage of early discovery, and to measure the mass in a model-independent way. We also expect that the MAOS invariant mass distribution can be used as a smoking-gun signal of the heavy resonance through its clear peak structure, which is generally less vulnerable to the background and momentum smearing effects.

TABLE I. The definition and the number of solutions of the MAOS schemes.

	Definition	Number of solutions	
		Events of M_{T2}^B	Events of M_{T2}^{UB}
MAOS1	Eqs. (22) and (23)	four-fold	four-fold
MAOS2	Eqs. (22) and (29)	unique	two-fold
MAOS3	Eqs. (22) and (30)	unique	unique

ACKNOWLEDGMENTS

The author would like to thank K. Choi and J. S. Lee for the initial collaboration and the fruitful discussion, and also J. M. Moreno and C. Papineau for useful comments on the manuscript. This work has been partially supported by Grants No. FPA2010-17747, Consolider-CPAN (CSD2007-00042) from the MICINN, HEPHACOS-S2009/ESP1473 from the C. A. de Madrid, and Contract UNILHC PITN-GA-2009-237920 of the European Commission.

[1] H. P. Nilles, Phys. Rep. **110**, 1 (1984); H. E. Haber and G. L. Kane, Phys. Rep. **117**, 75 (1985).

[2] N. Arkani-Hamed, A. G. Cohen, and H. Georgi, Phys. Lett. B **513**, 232 (2001); H. C. Cheng and I. Low, J. High Energy Phys. 09 (2003) 051.

[3] T. Appelquist, H. C. Cheng, and B. A. Dobrescu, Phys. Rev. D **64**, 035002 (2001).

[4] For a recent review, see A. J. Barr and C. G. Lester, J. Phys. G **37**, 123001 (2010).

[5] T. Han, I. W. Kim, and J. Song, Phys. Lett. B **693**, 575 (2010).

[6] E. L. Berger, Q. H. Cao, C. R. Chen, G. Shaughnessy, and H. Zhang, Phys. Rev. Lett. **105**, 181802 (2010); H. Zhang, E. L. Berger, Q. H. Cao, C. R. Chen, and G. Shaughnessy, Phys. Lett. B **696**, 68 (2011).

[7] L. M. Sehgal and M. Wanninger, Phys. Lett. B **200**, 211 (1988); J. Bagger, C. Schmidt, and S. King, Phys. Rev. D **37**, 1188 (1988); P. Ferrario and G. Rodrigo, Phys. Rev. D **80**, 051701 (2009); P. H. Frampton, J. Shu, and K. Wang, Phys. Lett. B **683**, 294 (2010); R. S. Chivukula, E. H. Simmons, and C. P. Yuan, Phys. Rev. D **82**, 094009 (2010); A. Djouadi, G. Moreau, F. Richard, and R. K. Singh, Phys. Rev. D **82**, 071702 (2010); Q. H. Cao, D. McKeen, J. L. Rosner, G. Shaughnessy, and C. E. M. Wagner, Phys. Rev. D **81**, 114004 (2010); M. Bauer, F. Goertz, U. Haisch, T. Pfoh, and S. Westhoff, J. High Energy Phys. 11 (2010) 039; C. H. Chen, G. Cvetic, and C. S. Kim, Phys. Lett. B **694**, 393 (2011); Y. Bai, J. L. Hewett, J. Kaplan, and T. G. Rizzo, J. High Energy Phys. 03 (2011) 003; J. A. Aguilar-Saavedra and M. Perez-Victoria, J. High Energy Phys. 05 (2011) 034; M. I. Gresham, I. W. Kim, and K. M. Zurek, Phys. Rev. D **83**, 114027 (2011); J. Shu, K. Wang, and G. Zhu, arXiv:1104.0083; A. Djouadi, G. Moreau, and F. Richard, Phys. Lett. B **701**, 458 (2011).

[8] L. Sonnenschein, Phys. Rev. D **73**, 054015 (2006); **78**, 079902(E) (2008); Y. Bai and Z. Han, J. High Energy Phys. 04 (2009) 056.

[9] H. Baer, M. Bisset, D. Dicus, C. Kao, and X. Tata, Phys. Rev. D **47**, 1062 (1993); H. Baer, M. Bisset, C. Kao, and X. Tata, Phys. Rev. D **50**, 316 (1994); F. Moortgat, S. Abdullin, and D. Denegri, arXiv:hep-ph/0112046; M. M. Nojiri, G. Polesello, and D. R. Tovey, arXiv:hep-ph/0312317; C. Charlot, R. Salerno, and Y. Sirois, J. Phys. G **34**, N1 (2007); G. Bian, M. Bisset, N. Kersting, Y. Liu, and X. Wang, Eur. Phys. J. C **53**, 429 (2008); M. Bisset, J. Li, and N. Kersting, arXiv:0709.1031; P. Huang, N. Kersting, and H. H. Yang, Phys. Rev. D **77**, 075011 (2008); M. Bisset, R. Lu, and N. Kersting, J. High Energy Phys. 05 (2011) 095.

[10] M. Bisset, J. Li, N. Kersting, R. Lu, F. Moortgat, and S. Moretti, J. High Energy Phys. 08 (2009) 037.

[11] H. C. Cheng, K. T. Matchev, and M. Schmaltz, Phys. Rev. D **66**, 036005 (2002); A. K. Datta, K. Kong, and K. T. Matchev, Phys. Rev. D **72**, 096006 (2005); **72**, 119901(E) (2005).

[12] A. J. Barr, B. Gripaios, and C. G. Lester, J. High Energy Phys. 07 (2009) 072.

[13] D. R. Tovey, J. High Energy Phys. 11 (2010) 148.

[14] A. J. Barr, S. T. French, J. A. Frost, and C. G. Lester, arXiv:1106.2322.

[15] W. S. Cho, K. Choi, Y. G. Kim, and C. B. Park, Phys. Rev. D **79**, 031701 (2009).

[16] K. Choi, S. Choi, J. S. Lee, and C. B. Park, Phys. Rev. D **80**, 073010 (2009); K. Choi, J. S. Lee, and C. B. Park, Phys. Rev. D **82**, 113017 (2010).

[17] J. Smith, W. L. van Neerven, and J. A. M. Vermaseren, Phys. Rev. Lett. **50**, 1738 (1983); V. D. Barger, A. D. Martin, and R. J. N. Phillips, Z. Phys. C **21**, 99 (1983).

[18] C. G. Lester and D. J. Summers, Phys. Lett. B **463**, 99 (1999); A. Barr, C. Lester, and P. Stephens, J. Phys. G **29**, 2343 (2003).

[19] A. J. Barr, B. Gripaios, and C. G. Lester, J. High Energy Phys. 11 (2009) 096; P. Konar, K. Kong, K. T. Matchev, and M. Park, J. High Energy Phys. 04 (2010) 086.

[20] C. Lester and A. Barr, J. High Energy Phys. 12 (2007) 102.

[21] W. S. Cho, K. Choi, Y. G. Kim, and C. B. Park, Phys. Rev. Lett. **100**, 171801 (2008); W. S. Cho, K. Choi, Y. G. Kim, and C. B. Park, J. High Energy Phys. 02 (2008) 035.

[22] C. G. Lester, J. High Energy Phys. 05 (2011) 076.

[23] D. R. Tovey, J. High Energy Phys. 04 (2008) 034; M. Serna, J. High Energy Phys. 06 (2008) 004.

[24] W. S. Cho, J. E. Kim, and J. H. Kim, Phys. Rev. D **81**, 095010 (2010); A. J. Barr, C. Gwenlan, C. G. Lester, and C. J. S. Young, Phys. Rev. D **83**, 118701 (2011); W. S. Cho, W. Klemm, and M. M. Nojiri, Phys. Rev. D **84**, 035018 (2011).

[25] B. Gripaios, J. High Energy Phys. 02 (2008) 053; A. J. Barr, B. Gripaios, and C. G. Lester, J. High Energy Phys. 02 (2008) 014.

[26] M. M. Nojiri and J. Shu, J. High Energy Phys. 06 (2011) 047.

[27] O. J. P. Eboli, C. S. Fong, J. Gonzalez-Fraile, and M. C. Gonzalez-Garcia, Phys. Rev. D **83**, 095014 (2011).

[28] M. Asano and Y. Shimizu, J. High Energy Phys. 01 (2011) 124.

[29] A. J. Barr and C. Gwenlan, Phys. Rev. D **80**, 074007 (2009); B. C. Allanach, A. J. Barr, A. Dafinca, and C. Gwenlan, J. High Energy Phys. 07 (2011) 104.

[30] B. C. Allanach, Comput. Phys. Commun. **143**, 305 (2002).

[31] T. Sjostrand, S. Mrenna, and P. Z. Skands, J. High Energy Phys. 05 (2006) 026.

[32] G. L. Bayatian *et al.* (CMS Collaboration), J. Phys. G **34**, 995 (2007).

[33] For example, see CDF Collaboration, CDF Note, Report No. 10436.

[34] E. L. Berger, Q. H. Cao, C. R. Chen, C. S. Li, and H. Zhang, Phys. Rev. Lett. **106**, 201801 (2011).